AGU PUBLICATIONS

Water Resources Research

RESEARCH ARTICLE

10.1002/2016WR020112

Chemical mass transport between fluid fine tailings and the overlying water cover of an oil sands end pit lake

Kathryn A. Dompierre[1], S. Lee Barbour[1], Rebecca L. North[2,3], Sean K. Carey[4], and Matthew B. J. Lindsay[5]

[1]Department of Civil and Geological Engineering, University of Saskatchewan, Saskatoon, Saskatchewan, Canada, [2]Global Institute for Water Security, University of Saskatchewan, Saskatoon, Saskatchewan, Canada, [3]Now at School of Natural Resources, University of Missouri, Columbia, Missouri, USA, [4]School of Geography and Earth Sciences, McMaster University, Hamilton, Ontario, Canada, [5]Department of Geological Sciences, University of Saskatchewan, Saskatoon, Saskatchewan, Canada

Key Points:
- First study of solute release from fluid fine tailings (FFT) stored under water cover in first oil sands end pit lake
- Mass balance confirmed constituents in FFT pore water largest mass input to water cover
- Numerical models show advection-dispersion during FFT settlement controls mass transport

Correspondence to:
K. Dompierre,
kathryn.dompierre@usask.ca

Citation:
Dompierre, K. A., S. Lee Barbour, R. L. North, S. K. Carey, and M. B. J. Lindsay (2017), Chemical mass transport between fluid fine tailings and the overlying water cover of an oil sands end pit lake, *Water Resour. Res.*, *53*, doi:10.1002/2016WR020112.

Received 12 NOV 2016
Accepted 12 MAY 2017
Accepted article online 17 MAY 2017

Abstract Fluid fine tailings (FFT) are a principal by-product of the bitumen extraction process at oil sands mines. Base Mine Lake (BML)—the first full-scale demonstration oil sands end pit lake (EPL)—contains approximately 1.9×10^8 m^3 of FFT stored under a water cover within a decommissioned mine pit. Chemical mass transfer from the FFT to the water cover can occur via two key processes: (1) advection-dispersion driven by tailings settlement; and (2) FFT disturbance due to fluid movement in the water cover. Dissolved chloride (Cl) was used to evaluate the water cover mass balance and to track mass transport within the underlying FFT based on field sampling and numerical modeling. Results indicated that FFT was the dominant Cl source to the water cover and that the FFT is exhibiting a transient advection-dispersion mass transport regime with intermittent disturbance near the FFT-water interface. The advective pore water flux was estimated by the mass balance to be 0.002 m^3 m^{-2} d^{-1}, which represents 0.73 m of FFT settlement per year. However, the FFT pore water Cl concentrations and corresponding mass transport simulations indicated that advection rates and disturbance depths vary between sample locations. The disturbance depth was estimated to vary with location between 0.75 and 0.95 m. This investigation provides valuable insight for assessing the geochemical evolution of the water cover and performance of EPLs as an oil sands reclamation strategy.

1. Introduction

The Canadian oil sands are the third largest known oil reservoir in the world, estimated to contain 166 billion barrels of oil [*Government of Alberta*, 2016]. Oil sands mining has disturbed more than 800 km^2 of land [*Government of Alberta*, 2014]; however, less than 1% of this area has received regulator certification as reclaimed [*Gosselin et al.*, 2010]. In addition, bitumen extraction from oil sands ore generates large volumes of tailings. More than 9.8×10^8 m^3 of fluid fine tailings (FFT) were stored in tailings impoundments by the end of 2013 [*Government of Alberta*, 2015].

Management and reclamation of FFT pose substantial geotechnical and environmental challenges. Associated pore waters exhibit elevated concentrations of dissolved inorganic chemical constituents, and organic compounds such as naphthenic acids, petroleum hydrocarbons, and unrecovered bitumen [*Allen*, 2008; *Dompierre et al.*, 2016; *Kavanagh et al.*, 2011]. Fluid fine tailings also exhibit high water content that persists for decades due to low settlement rates [*Kasperski and Mikula*, 2011]. At these high water contents, FFT behaves as a fluid and exhibits low shear strengths. A number of strategies are used to increase FFT strength, including flocculant and coagulant addition, large-scale centrifugation, thin-lift drying, and mechanical filtration [*Canada's Oil Sands Innovation Alliance Inc.* (*COSIA*), 2012a]. Treated FFT can be integrated into conventional terrestrial reclamation landscapes. However, these methods are expensive, time-consuming, and cannot accommodate daily FFT production.

End pit lakes (EPLs) offer long-term FFT containment with relatively low initial costs [*Cumulative Environmental Management Association* (CEMA), 2012]. These mine closure landscapes contain FFT deposits under a water cover within decommissioned mine pits. In the future, EPLs will be incorporated into the larger mine

closure landscape, and are expected to achieve sufficient water quality for release to natural systems [*CEMA*, 2012]. Thirty EPLs have been included in mine closure plans for the Athabasca oil sands region of Alberta, Canada. Half of these proposed EPLs will incorporate FFT below a water cover [*Prakash et al*., 2011].

The release of chemical constituents from the FFT will influence the long-term geochemical and biological evolution of an EPL [*Dompierre et al*., 2016]. Mass transport between the FFT and overlying water cover can occur via two key processes: (1) advection and hydrodynamic dispersion driven by FFT dewatering and elevated solute concentrations in FFT pore water [*Dompierre et al*., 2016]; and (2) FFT disturbance due to fluid movement in the water cover (e.g., internal waves) causing a rapid, but intermittent, mass release to the water cover [*Dompierre and Barbour*, 2016].

This study investigated water movement and chemical mass transport in the first EPL established in the Athabasca oil sands. Water and mass fluxes between the FFT and the water cover were assessed using a conservative tracer to evaluate the chemical mass balance of the EPL and to track mass transport within the FFT given field sampling and numerical modeling. Chloride (Cl) was selected as the conservative tracer as it is typically isolated from geochemical and biological reactions [*Feth*, 1981; *Weiner*, 2013]. Previous studies have used Cl to investigate groundwater flow and seepage to lakes [*Cox et al*., 2007; *Davis et al*.,1980; *Jacquet*, 1976; *Lee et al*., 1980], and to assess the mass balance of lakes [*Rimmer et al*., 2005; *Sacks et al*., 1998].

This investigation provides valuable insight for assessing the geochemical evolution of the water cover and performance of EPLs as an oil sands reclamation strategy. Results will assist in the development of monitoring and management plans for future EPLs. This study also provides insight on the potential for the mass flux over the FFT-water interface to change over time, as it can be compared to previous work on mass movement through the FFT at the first EPL [*Dompierre and Barbour*, 2016].

2. Materials and Methods

2.1. Study Site

Base Mine Lake (BML), the first full-scale demonstration EPL in the Athabasca oil sands region, was established at the Mildred Lake Mine, which is approximately 40 km north of Fort McMurray, Alberta, Canada (Figure 1). This region is located in a subhumid continental climate zone with long cold winters and short summers [*Carey*, 2008]. The mean annual temperature is 1.0°C and temperatures are below 0°C for 5–6 months of the year [*Environment Canada*, 2015].

Oil sands surface mining began at the Mildred Lake Mine in 1978. The oil sands ore is mined from the McMurray Formation, which contains on average 12% (w/w) bitumen (long chain hydrocarbons), 3–6% (w/w) water, and 84–86% (w/w) solids [*Chalaturnyk et al*., 2002]. Bitumen is extracted by adding hot water to reduce viscosity, sodium hydroxide to disperse clay particles, and aeration to promote bitumen flotation [*Caughill et al*., 1993; *Masliyah et al*., 2004]. The extracted bitumen is further upgraded to synthetic crude oil and the residual sand-clay slurry is hydrotransported to Mildred Lake Settling Basin (Figure 1). Following deposition in this tailings pond, the sand-sized particles quickly settle from the tailings slurry leaving a dense, warm fluid suspension called fluid fine tailings (FFT).

Fluid fine tailings pore water chemistry is dominated by oil sands process-affected water, which contains significant concentrations of dissolved ions (e.g., sodium, chloride, bicarbonate), naphthenic acids, petroleum hydrocarbons, and unrecovered bitumen [*Allen*, 2008; *Kavanagh et al*., 2011]. The initial FFT solids content is 25–35% (w/w), and is predominantly comprised of quartz and clay minerals including kaolinite, illite, chlorite, and illite-smectite [*Dompierre et al*., 2016; *Osacky et al*., 2013]. The residual bitumen content typically ranges from 1% to 6% (w/w) (G. Halferdahl, Syncrude Canada Ltd., personal communication, 2014). The FFT hydraulic conductivity is expected to range from 5×10^{-8} to 5×10^{-5} m s^{-1} based on typical FFT water content values and previous laboratory results [*Suthaker and Scott*, 1996].

Base Mine Lake was constructed within a decommissioned mine pit referred to as West In-Pit. Fluid fine tailings were dredged from Mildred Lake Setting Basin and pumped into the northeast corner of West In-Pit from 1994 to 2012. Throughout this period, BML was part of the recycle water circuit so a 3–5 m water cover was maintained over the FFT to provide water storage for various mining processes. This mine closure landscape was commissioned as an EPL in November 2012. At this time, the maximum FFT depth in BML was 45 m, corresponding to a total FFT volume of approximately 1.9×10^9 m^3. The average FFT temperature is approximately

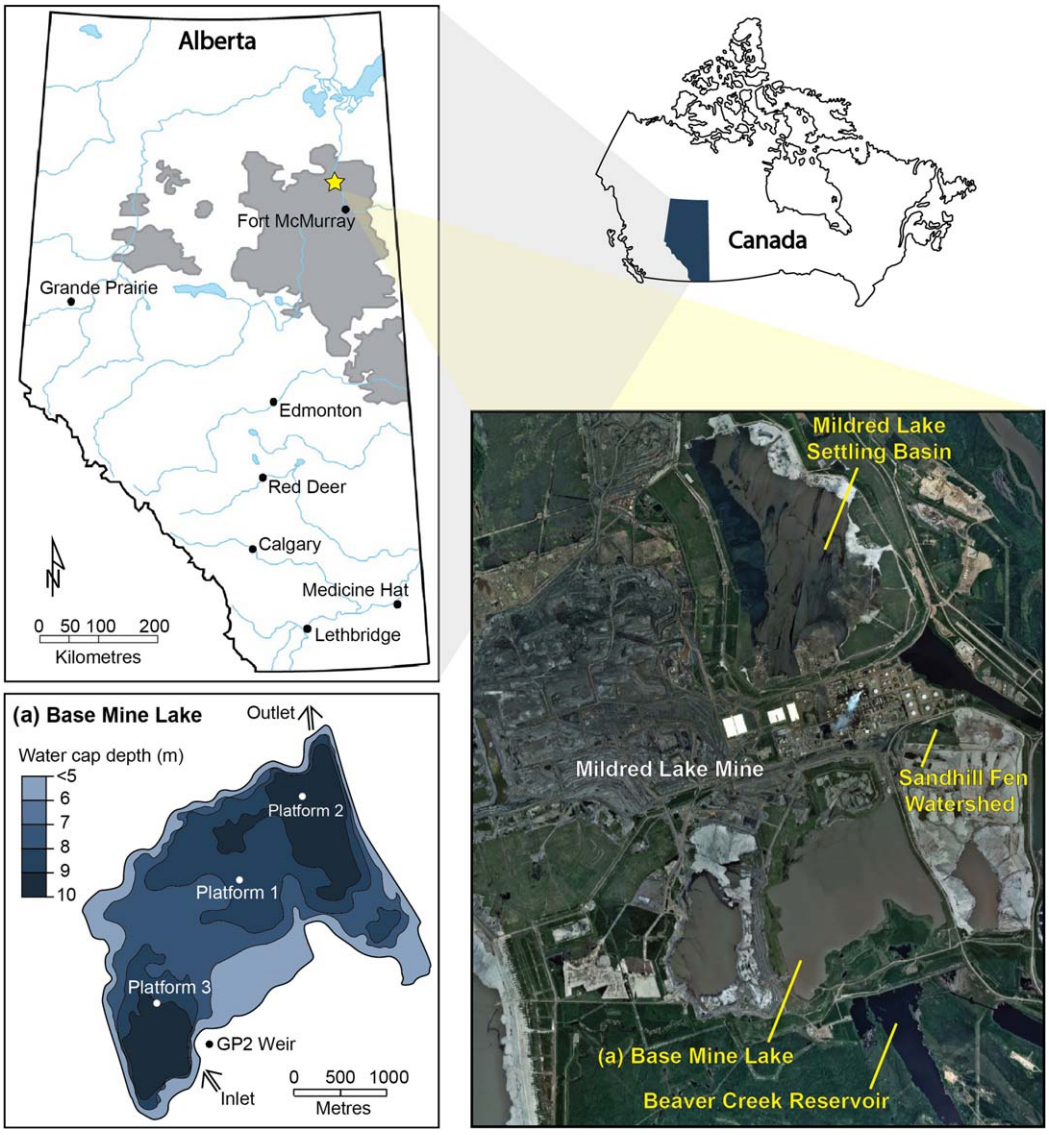

Figure 1. Mildred Lake Mine location (starred) relative to known oil sands deposits (gray shaded areas) and aerial photo of the site; inset (a) shows the BML monitoring locations and water cover depth in June 2013.

13°C [*Dompierre et al.*, 2016]. After commissioning, freshwater was pumped into BML from Beaver Creek Reservoir (Figure 1) during ice-free months. Water was concurrently pumped out of BML—for use in the bitumen extraction process—to maintain a lake surface elevation of 308.5 $\pm$ 0.5 m above sea level (masl). The average water cover depth was 8.5 m at the beginning of 2013. In October 2015, near the end of the study period, the estimated water cover volume was 5.8×10^7 m^3 with a surface area of approximately 7.8 km^2.

The water cover responds to seasonal temperature cycles in a similar manner as natural temperate, northern lakes [*Lawrence et al.*, 2016; *Oswald and Rouse*, 2004; *Rouse et al.*, 2003]. During the summer months, the water cover is thermally stratified from the end of May to the beginning of September. The epilimnion (upper portion of the water cover) temperature increases throughout June to 20°C and stays at this temperature until September. Concurrently, the hypolimnion (lower portion of the water cover) gradually warms to 15°C. In the fall, the water cover is fully mixed from the beginning of September until ice forms in November. Over the winter season, the water column exhibits inverse stratification below the ice cover. Temperatures remain relatively constant throughout this period with water near the ice at 0°C and a temperature of 4°C near the FFT-water interface. The ice cover melts by the end of April, which is followed by a weaker and more irregular spring turnover, as compared to the fall turnover [*Lawrence et al.*, 2016].

The FFT is currently undergoing hindered settlement or self-weight consolidation [*Canada's Oil Sands Innovation Alliance Inc.* (*COSIA*), 2012b], which means that the FFT near the pit bottom dewaters first, with the expressed pore water creating a vertical pore water flux through the FFT. Pore water movement is generally expected to be upward due to the relatively low hydraulic conductivity of the underlying formations. Clearwater Formation shales and siltstones form the BML pit and exhibit a mean vertical hydraulic conductivity of 8×10^{-10} m s^{-1} (D. Heisler, Syncrude Canada Ltd., personal communication, 2015). Initial FFT settlement would have occurred during the first few years after deposition; however, high water contents are expected to persist for an extended time period [*Kasperski and Mikula*, 2011]. These slow settlement rates are due to the addition of dispersants (sodium hydroxide) during bitumen extraction and naturally occurring surfactants (asphaltic acids) present in the ore that are released during heating [*Chalaturnyk et al.*, 2002; *Jeeravipoolvarn et al.*, 2009].

A preliminary FFT consolidation model, developed to evaluate the long-term settlement in BML, estimated settlement rates of approximately 1 m a^{-1} after deposition, decreasing exponentially over 30 years to approximately 0.1 m a^{-1} [*Carrier et al.*, 2007]. A field study by *Dompierre and Barbour* [2016] found that the FFT settlement generated an upward pore water flux of 0.004 m^3 m^{-2} d^{-1} (1.5 m^3 m^{-2} a^{-1}) approximately 1 year after BML was commissioned.

Two approaches were used to assess chemical mass flux from the FFT to the overlying water cover, both of which used Cl as a conservative tracer. The first evaluated the Cl mass balance within the water cover to determine the conservative mass flux from FFT. The chemical mass balance included an initial assessment of the water balance within the water cover, and a field sampling campaign to characterize the Cl concentrations of BML and all inflow and outflow waters. The second investigated the mechanisms controlling mass transport within the FFT, using pore water Cl concentrations to develop numerical models for predicting mass movement across the FFT-water interface.

2.2. Sample and Data Collection

A field investigation evaluated the volumes and mass associated with the input and output waters at BML. Water and mass inputs included water pumped in from Beaver Creek Reservoir, precipitation (snow and rain), runoff from the surrounding watershed, and pore water released from the underlying FFT. Outputs included water and mass pumped from the water cover for use in the processing plant, and water loss due to evaporation. Groundwater interactions with the water cover were assumed negligible due to the relatively low hydraulic conductivity of the formation surrounding the pit.

The water volume pumped into and out of BML each day was monitored with Rosemount magnetic flowmeters (accuracy of $\pm$0.25%, Emerson Process Management, Shakopee, MN, USA). The water cover surface elevation was measured using GPS, while sonar surveys, completed in October of each year, verified the FFT-water interface elevation.

Rainfall volumes were monitored with three unobstructed CS700 tipping-bucket rainfall gauges (Campbell Scientific, Edmonton, AB, Canada) located at the adjacent Sandhill Fen Watershed (Figure 1). Snowfall was estimated using the mean value from three CS725 snow water equivalent sensors (Campbell Scientific, Edmonton, AB, Canada) corroborated with annual snow surveys at Sandhill Fen. These values were compared with snow water equivalent data reported by Environment Canada at the Mildred Lake weather station [*Environment Canada*, 2015]. The Sandhill Fen likely accumulates more snow as water equivalent than BML as it is more sheltered; however, both environments are subject to wind redistribution. Runoff volumes from the contributing watershed were measured at a weir on the south side of BML (GP2 weir; Figure 1). The observed runoff volumes were assumed to be representative of the entire terrestrial watershed, which covers a 6.6 km^2 area or approximately 80% of the water cover surface area.

Evaporation from the water cover was measured using the eddy covariance technique [*Aubinet et al.*, 2012]. The eddy covariance system involved a LI-7200 enclosed path infrared gas analyzer (LI-COR, Lincoln, NE, USA) and R3–50 3-D sonic anemometer (Gill Instruments Ltd., Lymington, UK), and was installed in the center of BML at Platform 1 (Figure 1). Wind speed and water vapor concentrations were measured at 10 Hz and covariances were computed for 30 min intervals using EddyPro® LI-COR. During short periods ($<$2 h) when the system was not working, evaporation was estimated using linear interpolation. For longer periods,

a monthly logistic regression model was developed for evaporation as a function of net radiation, wind speed, and vapor pressure deficit measured at Platform 1 to provide continuous data.

Samples of the BML water cover were frequently collected between May 2013 and October 2015. The samples were collected biweekly during the open water season, and once under the ice in the winter. Water samples were collected at several stations around BML (Platforms 1, 2, and 3; Figure 1). Inflow and outflow samples were also obtained during routine sampling when the pumps were in operation. Rainfall samples were collected from five locations around the BML perimeter in the fall of 2015, while snow samples were obtained at 10 locations over the frozen water cover surface in March 2015. Runoff at the GP2 weir was sampled during the spring melt period (18 March to 3 June 2014; 27 March to 15 April 2015). All water samples were collected into HDPE bottles and sealed with no headspace. The samples were chilled at 4°C until they were analyzed at a commercial laboratory. The Cl concentrations were quantified by ion chromatography (EPA Method 300.0) on samples passed through 0.45 μm polyethersulfone membranes.

Tailings (and water) samples were obtained at high-spatial resolution across the FFT-water interface at Platforms 1, 2, and 3 (Figure 1) on 4 and 5 August 2015. These samples were collected with a custom-built fixed interval sampler deployed using a boat-mounted overhead winch and pulley system. This sampler was comprised of 20 discrete sampling cylinders positioned at 0.1 m depth intervals. Each cylinder contained a pneumatically controlled piston with a 250 mL total displacement volume. Compressed nitrogen gas (275 kPa) was used to maintain the pistons in the closed position while the sampler was slowly lowered to the FFT-water interface. Five cylinders were positioned above and fifteen below the FFT-water interface, which was first determined by active sonar [*Dompierre et al.*, 2016]. After a 10 min settlement period, the compressed nitrogen was evacuated from the cylinders into the sampler lines, and the pistons retracted to the open position using a vacuum pump. After approximately 5 min, the sampler was retrieved to surface, one 250 mL HDPE bottle was threaded onto each cylinder, and the samples were extruded using compressed nitrogen to move the pistons back to the closed position. Pore water was extracted from FFT solids by centrifugation at 10,000 rpm for 30 min and passed through 0.45 μm polyethersulfone membranes. The pore water samples were stored in HDPE bottles with zero headspace and refrigerated at 4°C until the Cl concentrations were quantified by ion chromatography (EPA Method 300.0).

2.3. Mass Balance Calculations

An annual water balance was completed for the entire BML system (FFT and water cover; Figure 2) from 1 November 2013 to 31 October 2014 (Period 1) and 1 November 2014 to 31 October 2015 (Period 2). The measured elevation change of the water surface was compared to the calculated net water flux over the water surface, dS (m^3 or mm), determined by:

$$dS = I_W - O_W = V_{p_{in}} + V_{prec} + V_{ro} - V_{evap} - V_{p_{out}} \quad (1)$$

where I_W is the total water volume (depth) contributed to BML from the inputs (pump-in water, $V_{p_{in}}$; precipitation, V_{prec}; and runoff, V_{ro}) and O_W is the total volume (depth) removed by the outputs (pump-out water, $V_{p_{out}}$; and evaporation, V_{evap}). Pore water release from the FFT was not considered to be an input for the above water balance calculation as it does not affect the water surface elevation but instead causes the elevation of the water cover bottom (FFT-water interface) to drop over time. Water movement over the pit walls and base was assumed to be negligible.

The change in Cl stored in the water cover was calculated for the same two periods as the annual water balances (1 November 2013 to 31 October 2014; 1 November 2014 to 31 October 2015) using the following equation:

$$dM = I_M - O_M = M_{p_{in}} + M_{prec} + M_{ro} + M_{pw} - M_{p_{out}} \quad (2)$$

where dM represents the change in Cl stored in the lake (g), I_M, is the total mass of Cl associated with the inputs (FFT pore water, M_{pw}; pump-in water, $M_{p_{in}}$; precipitation, M_{prec} and runoff, M_{ro}). The total mass removed from the lake due to outputs, O_M, was the mass associated with the pump-out water ($M_{p_{out}}$). The product of the volume, V (m^3), and Cl concentration, C (g m^{-3} or mg L^{-1}), of each input or output (except for the FFT pore water) was used to determine its associated chemical mass. Pore water released by the FFT was not directly measured and represents an unknown in the above equation (and in Figure 2). Mass

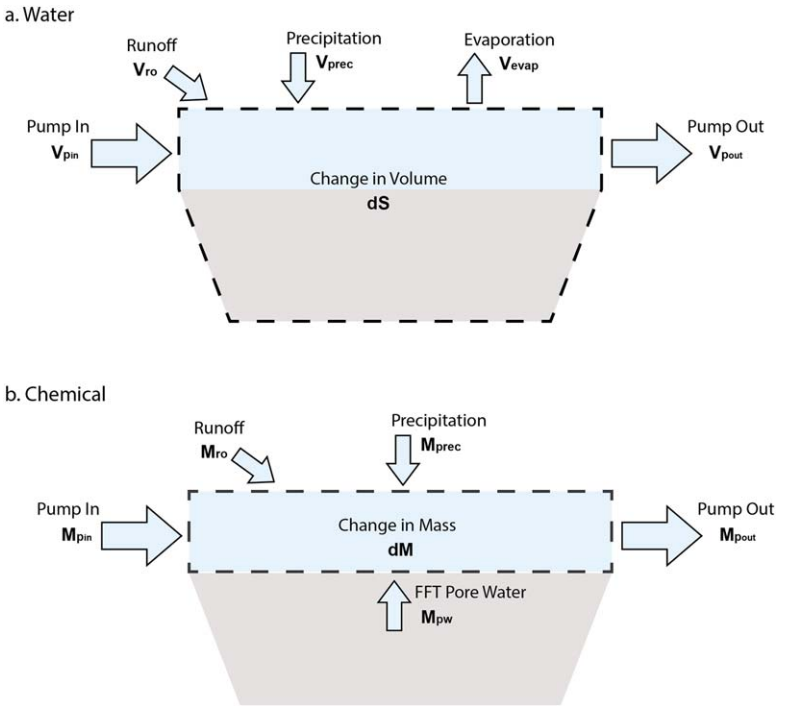

Figure 2. Inputs, outputs, and the domain (outlined by the thick dashed line) associated with the (a) water and (b) chemical mass balances.

exchange over the pit walls was assumed to be negligible as the pit wall surface area is relatively small compared to the FFT surface.

The Cl in the lake at the beginning and end of each period was calculated with the average concentration throughout the whole water cover, multiplied by the water cover volume at the specified time. Thus, the change in Cl stored in the lake, *dM*, was calculated by:

$$dM = V_{L_2} C_{L_2} - V_{L_1} C_{L_1} \tag{3}$$

where V_L is the lake volume and C_L is the volume-weighted average Cl concentration in the lake at the beginning (1) and end (2) of the mass balance period. The water cover volume was determined from the water surface elevation, FFT-water interface elevation data, and pit capacity curves describing the volume below a given elevation.

The mass released by the FFT, M_{pw}, was determined by rearranging equation (2) to:

$$M_{pw} = (V_{L_2} C_{L_2} - V_{L_1} C_{L_1}) - V_{p_{in}} C_{p_{in}} - V_{prec} C_{prec} - V_{ro} C_{ro} + V_{p_{out}} C_{p_{out}} \tag{4}$$

and the average Cl mass flux from the FFT (g m^{-2} s^{-1}) was calculated by dividing the Cl released from the FFT (M_{pw}) by the area associated with the FFT-water interface and the total time (1 year). This area is expected to change as FFT settles due to the sloping pit walls in BML. The FFT surface area was determined from FFT-water interface elevation data and pit capacity curves describing the cross-sectional area of the BML pit with elevation.

A sensitivity analysis was conducted to evaluate which assumptions and inputs to the mass balance equation were most likely to influence the calculated FFT mass flux. The sensitivity analysis considered the water cover volume, which was affected by both the water surface and FFT-water interface elevation, the surface area of the FFT contributing to mass release, and the concentrations associated with the water cover, precipitation, runoff, pump-in, and pump-out waters. The baseline used for the sensitivity analysis was the original mass balance calculation. Each input was altered over a range of expected values while all other values remained the same as the baseline case. The range of values used for each input was based on the expected error associated with its measurement. The maximum and minimum FFT mass fluxes calculated with each range were compared to the baseline FFT mass flux.

2.4. Numerical Modeling

One-dimensional mass transport models for advection and hydrodynamic dispersion (or advection-dispersion) were developed using a commercial finite element simulation software for ground water flow and mass transport [CTRAN/W, *GEO-SLOPE International Ltd*., 2012; SEEP/W, *GEO-SLOPE International Ltd*., 2013]. The model domain was a 5 m FFT column with continuously changing volumetric water content with depth, to represent the variation in solids content observed in the field [*Dompierre and Barbour*, 2016]. The model domain depth was sufficient to capture the observed transition of pore water concentrations from typical FFT signatures to that of the overlying water cover [*Dompierre and Barbour*, 2016]. This region is also expected to have a relatively consistent pore water flux rate as pore water flow is primarily generated from the bottom of the FFT deposit during preliminary self-weight consolidation. Consolidation was assumed to have a negligible effect on the FFT properties within this region over the simulated period.

The initial and boundary conditions were set as normalized concentrations based on the Cl values measured in the field. The general formula for calculating the normalized concentration, C_n, is:

$$C_n = \frac{C - C_{\min}}{C_{\max} - C_{\min}} \tag{5}$$

where $C_{\min}$ and $C_{\max}$ represent the minimum and maximum observed concentrations, respectively. The value used for $C_{\min}$ was the minimum Cl value observed in the water cover, corresponding to a normalized concentration of 0.0. The value used for $C_{\max}$ was the average Cl concentration within the deep FFT pore water at each location, corresponding to a normalized concentration of 1.0. Thus, the initial concentration in the FFT was set to a normalized value of 1.0, as was the lower boundary of the modeled domain. The upper boundary condition changed over time based on the results from the lake water chemistry sampling program.

The model was set to begin in May 2013, when freshwater pumping began, and continued until October 2015. In each simulation, a mass transport regime (i.e., diffusion only or advection-dispersion) was maintained throughout the modeled time period. The upward water fluxes applied to the advection models ranged from 0.0005 to 0.01 $m^3\ m^{-2}\ d^{-1}$. These values were based on the 2013 and 2014 FFT dewatering rates determined by the FFT-water interface sonar surveys and previous tracer work at BML [*Dompierre and Barbour*, 2016].

The coefficient of molecular diffusion was estimated using the volumetric water content of the FFT with depth, and the relationship between porosity and the diffusion coefficient established by *Boudreau* [1996]. The free water diffusion coefficient for Cl was taken from *Cussler* [1997] and was modified based on the average in situ FFT temperature (10°C) after *Li and Gregory* [1974]. The volumetric water content varied from 86% to 82%, and the associated diffusion coefficients ranged from 7.8×10^{-10} to $6.6 \times 10^{-10}\ m^2\ s^{-1}$.

Longitudinal dispersivity was included in the models and was assumed to be 0.01 times the plume length [*Kamp et al*., 1994; *Gelhar et al*., 1992]. The plume length was observed to be 0.4 m, corresponding to the depth over which the Cl concentrations transitioned from average FFT pore water values to average water cover values. The linear pore water velocities, calculated by dividing the water flux by the volumetric water content of the top FFT layer (porosity), were found to range from 0 to $1.4 \times 10^{-7}\ m\ s^{-1}$. The assumed dispersivity value and the calculated pore water velocities produced a range in values for the coefficient of mechanical dispersion from 0 to $1.4 \times 10^{-9}\ m^2\ s^{-1}$.

Additional model scenarios were developed to simulate a disturbance within the top portion of the FFT during the fall turnover. Two disturbance depths, 0.5 and 1 m, were added to the model by changing the FFT pore water concentration in the disturbed zone to the water cover concentration immediately before the disturbance events (15 October 2013 and 15 October 2014). These model scenarios were developed to evaluate previous evidence of FFT disturbance provided by stable isotopes of water and temperature profiles measured in BML [*Dompierre and Barbour*, 2016].

The simulated concentration profiles were independently compared to the normalized Cl concentrations associated with each sample location (from 4 and 5 August 2015). The root-mean-square error (RMSE) between each modeled scenario and the field results was calculated to provide a preliminary estimate for the model providing the best fit. The numerical models were also used to investigate mass flux rates over the FFT-water interface and cumulative mass released from the FFT given the simulated advection-dispersion transport regimes.

Table 1. Water Volume and Mass of Cl Associated With Each Input (+) and Output (−)

	Period 1[a]			Period 2[b]		
Input/ Output	Depth (mm)	Volume ($\times 10^6$ m^3)	Cl Mass ($\times 10^6$ g)	Depth (mm)	Volume ($\times 10^6$ m^3)	Cl Mass ($\times 10^6$ g)
Rain	309	2.38	1.9	254	1.96	1.3
Snow	55	0.42	0.1	50	0.39	0.2
Runoff	29	0.23	2.5	21	0.16	1.4
Pump In	852	6.56	22.4	780	6.01	16.4
Pump Out	−955	−7.35	−2895.7	−953	−7.34	−2609.4
Evaporation	−351	−2.70		−351	−2.70	

[a]Period 1: 1 November 2013 to 31 October 2014.
[b]Period 2: 1 November 2014 to 31 October 2015.

3. Results

3.1. Water and Chemical Balance

Pumping from Beaver Creek Reservoir represented the largest water input to BML during both sampling periods (Table 1). The pump was operated from May to October and contributed more than 6×10^6 m^3 of water to BML each year. This volume is approximately 10% of the total water cover volume and corresponds to a water depth greater than 780 mm when normalized to the BML surface area (by dividing by the area: 7.7×10^6 m^2). Rainfall was the next largest water input, followed by snow and runoff.

The largest water withdrawal was associated with pumping, which accounted for a larger water volume than pumping inputs from Beaver Creek Reservoir. Evaporation from the lake surface was very similar over the two measurements periods, even though the monthly evaporation rates differed between Period 1 and Period 2. The evaporation rates measured in 2014 and 2015 were considerably less than calculated open-water potential evaporation [*Penman*, 1948] and were lower than values determined for natural lakes in the same region [*Ferguson et al.*, 1970; *Blanken et al.*, 2000].

A net water loss was determined for both of the water balance periods (60 mm in Period 1 and 198 mm in Period 2). The water loss generally corresponded to the measured surface elevation changes of 50 mm in Period 1 and 240 mm in Period 2. Temporal trends in calculated storage and measured water cover surface level were generally similar (Figure 3). Uncertainty associated with the water balance was due to sampling error (rain, snow, and runoff samples), instrumentation error (pump in and pump out flowmeters, evaporation eddy covariance system, and rain gauges), and sample representation (rain, snow, runoff, and evaporation samples). Pumped water represents the largest flow in and out of BML, and was assumed to be the largest contributor to water balance uncertainty. The pumps shut off when the associated flowmeter stopped working so uncertainty of the pumped water was only due to instrumentation error. Uncertainty of these measurements would be approximately $\pm 0.016 \times 10^6$ m^3 for the pump in and $\pm 0.018 \times 10^6$ m^3 for the pump out volumes, given the flowmeter accuracy (±0.25%).

The average runoff Cl concentration was 19.2 mg L^{-1} in Period 1 and 8.8 mg L^{-1} in Period 2; while the average rain and snow Cl concentrations were 0.82 and 2.25 mg L^{-1}, respectively, measured over both periods. Chloride inputs from precipitation and runoff were relatively small compared to the mass contributed from the pumps (Table 1), even though this water had relatively low average concentrations of 3.3 mg L^{-1} in Period 1 and 3.1 mg L^{-1} in Period 2. The pump out water had an average concentration of 449.2 mg L^{-1} in Period 1 and 410.4 mg L^{-1} in Period 2. The Cl mass associated with the pump out water was at least an order of magnitude greater than the combined contributions from precipitation, runoff, and the pump in water.

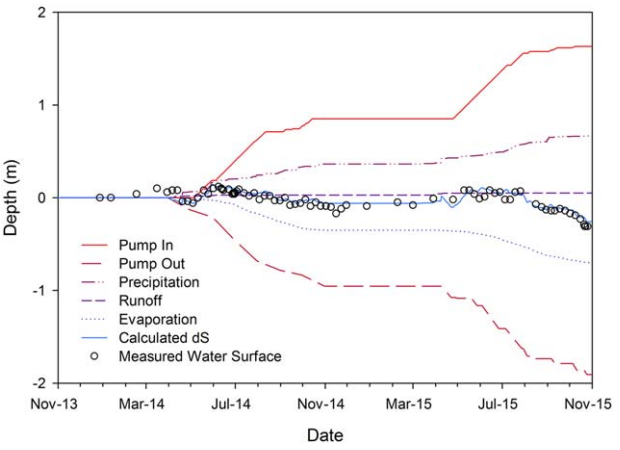

Figure 3. Cumulative annual water balance for Period 1 and Period 2 with the measured inputs and outputs (dashed lines), the calculated cumulative change in surface elevation (thick blue line) and measured cumulative change in water surface elevation (circles).

The Cl concentrations in the water cover, averaged from the multiple sampling locations, decreased over time (Figure 4). The initial water cover Cl concentration

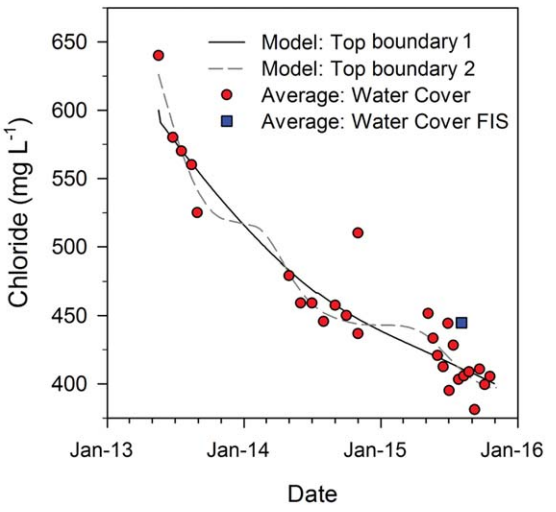

Figure 4. Average water cover Cl concentrations from the long-term chemistry sampling program (circles) and collected near the bottom of the water cover by the fixed interval sampler (square; labeled FIS); water cover concentration trends (solid and dashed lines) used for the upper boundary condition in the numerical models.

was 640 mg L^{-1} in May 2013. This value was similar to Cl concentrations in oil sands process water measured at the Mildred Lake mine site [*Allen*, 2008; *Dompierre et al*., 2016]. The initial water cover chemical composition was typical of process water because this system was part of the recycle water circuit up until being commissioned as an EPL. The average water cover Cl concentration decreased from greater than 600 mg L^{-1} to approximately 400 mg L^{-1} by the fall of 2015, primarily due to freshwater inputs from Beaver Creek Reservoir. Small fluctuations in the water cover Cl concentration were observed over the monitored period, likely due to transient changes in evaporation rates or pumping, and possibly due to seasonal stratification of the water cover. The yearly mass balance method was chosen, as opposed to a monthly or daily mass balance, to limit the uncertainty associated with this seasonal variability.

The water cover volume varied within Periods 1 and 2 due to changes in the water surface elevation and the FFT-water interface. The water cover volume increased from 5.1 $\times$ 10^7 m^3 to 5.6 $\times$ 10^7 m^3 during Period 1 and to 5.9 $\times$ 10^7 m^3 by the end of Period 2. A concomitant decrease in the FFT-water interface elevation also caused the FFT surface area contributing to pore water release to decrease due to a slight narrowing of the pit with depth. The cross-sectional area associated with the FFT-water interface was estimated to be approximately 6.5 $\times$ 10^6 m^2 in November 2013, 6.4 $\times$ 10^6 m^2 in November 2014, and 6.3 $\times$ 10^6 m^2 in November 2015.

Based on the change in mass stored in the water cover and the mass inputs and outputs over the two measurement periods, the calculated mass contribution from the FFT was 1.9 $\times$ 10^9 g in Period 1 and 1.8 $\times$ 10^9 g in Period 2. Given the average FFT-water interface surface area during each period, the mass released from the FFT was 300 g m^{-2} in Period 1 and 280 g m^{-2} in Period 2. These values are associated with estimated mass fluxes of 0.81 g m^{-2} d^{-1} (Period 1) and 0.76 g m^{-2} d^{-1} (Period 2) from the FFT to the overlying water cover. This mass flux represented the largest chemical loading to the water cover each year, as it was approximately 99% of the total mass inputted to BML in both periods.

The sensitivity analysis illustrated that the calculated mass flux from the FFT was not significantly affected by variability in the input and output water concentrations nor changes to the FFT surface area contributing to the mass loading (Table 2). The mass balance calculations were most sensitive to the mass stored in the water cover at the beginning and end of the mass balance periods. The variability associated with the water cover volume and concentration, both used to determine the stored mass, caused the largest shift in the calculated FFT mass input. The sensitivity analysis suggests that the potential mass flux from the FFT could vary from 0.5 to 1.1 g m^{-2} d^{-1} in Period 1 and 0.5 to 1.0 g m^{-2} d^{-1} in Period 2.

3.2. Mass Transport Modeling

High-resolution depth profiles of Cl concentrations across the FFT-water interface were similar among the three sampling locations (Figure 5). Concentrations at the FFT-water interface were consistent with Cl values in the overlying water cover. However, Cl concentrations transition to a value representative of deeper FFT pore water within 0.5 m from the FFT-water interface. The transition zone depth was similar to that observed for the stable isotopes of water [*Dompierre and Barbour*, 2016].

The Cl concentrations in the water cover near the FFT-water interface were also consistent among the three sample locations (Platforms 1, 2, and 3; Figure 1) with an average value of 440 mg L^{-1} and a standard deviation of 8.2 mg L^{-1}. These values were slightly higher than the average Cl concentration measured by the long-term water cover chemistry sampling program in August 2015 (Figure 4). The values obtained were

Table 2. Sensitivity Analysis Ranges and Associated Percent Change in Calculated FFT Mass Input to the Water Cover

	Sensitivity Analysis Range		Change in Calculated FFT Mass Input[d]	
Input	Period 1	Period 2	Period 1	Period 2
Water cover volume (m^3)	±657,000[a]	±650,000[a]	±32.9	±27.9
FFT surface area (m^2)	±200,000[a]	±200,000[a]	±3.1	±3.1
Lake concentration (mg L^{-1})	±10[a]	±10[a]	±26.5	±31.6
Input Concentrations				
Rain (mg L^{-1})	0.2–6.0[b]	0.2–6.0[b]	−0.6 to 0.1	−0.4 to 0.1
Snow (mg L^{-1})	0.1–3.0[c]	0.1–3.0[c]	±0.0	±1.0
Runoff (mg L^{-1})	5.8–53.4[a]	5.8–53.4[a]	−0.3 to 0.1	−0.4 to 0.0
Pump in (mg L^{-1})	±1[a]	±1[a]	±0.3	±0.3
Pump out concentration (mg L^{-1})	±10[a]	±10[a]	±3.3	±3.6

[a]Based on the observed variability or uncertainty associated with the field measurements.
[b]According to field measurements conducted at a nearby reclamation site (J. Price, University of Waterloo, personal communication, 2016).
[c]After snowpack Cl concentrations measured by *Murray* [1981].
[d]Expressed as a percent of the originally calculated FFT mass input.

likely higher because the sample was collected from the region just above the FFT-water interface during summer stratification. This region would be affected by FFT pore water release during this stable period, whereas the top layer generally exhibits lower electrical conductivity.

The pore water concentrations greater than 0.5 m below the FFT-water interface varied between sample locations; 580 ± 12 mg L^{-1} at Platform 1, 600 ± 18 mg L^{-1} at Platform 2, and 640 ± 19 mg L^{-1} at Platform 3. These values were consistent with water cover concentrations measured in May 2013, before substantial freshwater addition occurred (Figure 4). The pore water concentrations below 1.5 m were slightly lower than those between 0.5 and 1.5 m. This suggests that pore water Cl concentrations may have increased with time as FFT was placed in BML. A general enrichment of oil sands process water, which constitutes the FFT pore water, has been observed due to water reuse for the bitumen extraction process through the recycle water circuit [*Baer*, 2014; *Baer and Barbour*, 2013].

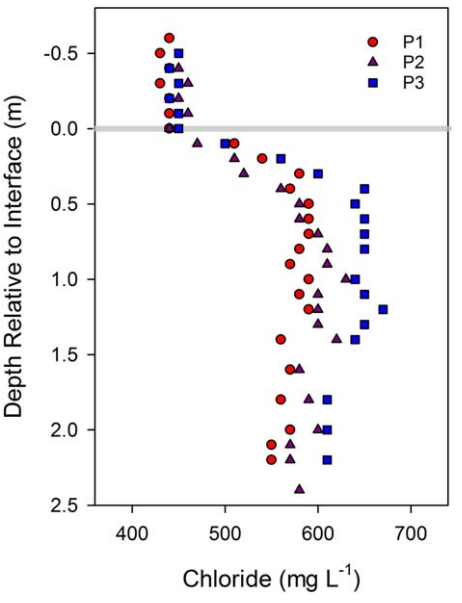

Figure 5. Depth profiles of dissolved Cl concentrations for FFT samples collected in August 2015 at the three platforms (P). Depths are presented relative to the FFT-water interface, which is denoted by the solid horizontal line.

A continuously decreasing concentration was specified at the top of the modeled profile (Figure 4, top boundary 1) to reflect the water cover concentration trends measured by the long-term sampling program. The numerical model with a diffusion-only mass transport regime and no FFT disturbance produced a 0.7 m transition depth; however, when an advective flux was added to the models, the transition zone depth decreased (Figure 6). Pore water advection carries mass from the underlying FFT upward and consequently, as advection increases, mass spreading over the FFT-water interface via diffusion declines. This trend was similar for the simulations with FFT disturbance; however, the transition zone depth also increased with disturbance depth. The transition zone increased with the simulated disturbance depth because mixing of the FFT and water cover caused the Cl concentrations to decrease within the disturbed FFT. Advection rates of 0.006–0.010 $m^3\ m^{-2}\ d^{-1}$ produced very similar Cl profiles within the FFT for all modeled disturbance depths.

The measured Cl profiles were normalized based on the average FFT pore water concentration at each location and the minimum concentration measured in the water cover (380 mg L^{-1}). The normalized concentration

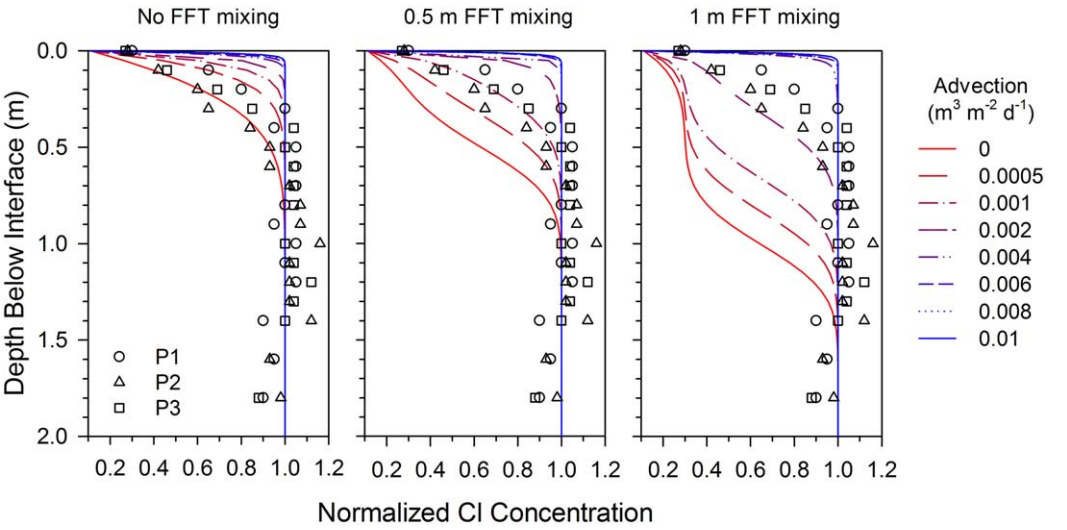

Figure 6. Normalized Cl concentrations from the field measurements at the three platforms (P) and simulated advection-dispersion transport regimes with top boundary 1 and three disturbance depths (0, 0.5, and 1 m) generated for the final sampling date (5 August 2015).

profiles were compared to the simulation results (Figure 6 and Table 3). The RMSE values determined for the simulations with advection rates of 0.008 and 0.010 $m^3\ m^{-2}\ d^{-1}$ were not included in Table 3 as they were similar to the values provided for 0.006 $m^3\ m^{-2}\ d^{-1}$.

The pore water flux providing the best fit to the field data was not the same for all platforms for a given disturbance depth. In general, the lowest RMSE for Platform 1 was associated with a greater pore water flux than the best fit scenarios for Platforms 2 and 3. The FFT-water interface sonar surveys detected differential settlement around BML, revealing that FFT pore water movement likely varies with location. For example, the FFT-water interface exhibited the greatest elevation change in the northeast corner of BML, where Platform 2 is located (Figure 1). Thus, greater pore water flux was expected at Platform 2 when compared to the other sample locations.

The FFT-water interface sonar surveys also indicated that a diffusion-only mass transport regime is unlikely given the measured FFT settlement. The modeled scenarios with a 0.5 or 1 m disturbance generally corresponded to these field observations. Evidence of FFT disturbance was observed in the field as the water cover turbidity exhibited a rapid increase during unstable periods in the lake when the water column was completely mixed [*Lawrence et al.*, 2016]. Disturbance within the FFT was also supported by the previous tracer study [*Dompierre and Barbour*, 2016].

The modeled scenarios were rerun with an alternate top boundary condition (top boundary 2; Figure 4) to determine the sensitivity of the simulations to the water cover concentration. This boundary condition was generated in the models using an approximate spline function based on the long-term Cl field measurements. The Cl profiles generated by these modified models were similar to the original results (Figure 6), and did not alter the modeled scenarios providing the best fit to the field data.

Table 3. RMSE (%) for Each Modeled Scenario Compared to Field Concentrations at Each Platform (P)

Advective Flux ($m^3\ m^{-2}\ d^{-1}$)	No. FFT Mixing			0.5 m FFT Mixing			1 m FFT Mixing		
	P1	P2	P3	P1	P2	P3	P1	P2	P3
0	12.5	7.8[a]	8.8[a]	29.4	18.2	26.2	49.2	41.9	46.9
0.0005	7.1[a]	13.9	9.7	19.0	9.3	15.0	42.7	34.0	40.9
0.001	9.2	17.7	13.9	9.7[a]	8.9[a]	7.4[a]	35.4	25.2	33.2
0.002	11.4	20.1	16.8	10.2	18.8	15.2	17.0	8.2[a]	13.4[a]
0.004	12.1	20.8	17.6	12.1	20.8	17.6	11.8[a]	20.5	17.2
0.006	12.2	20.8	17.7	12.2	20.8	17.7	12.2	20.8	17.7

[a]The lowest RMSE, indicating the calculated best fit.

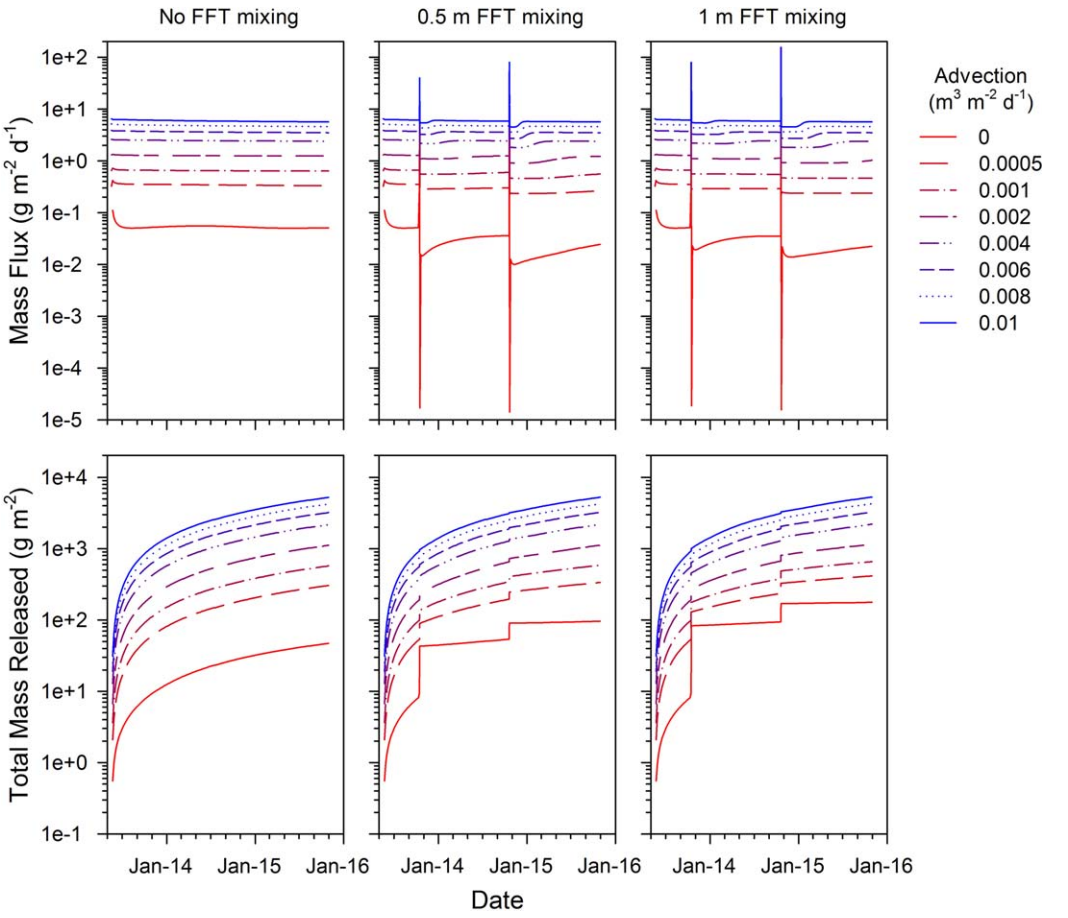

Figure 7. Chloride flux rates over the FFT-water interface and cumulative mass released from the FFT starting in May 2013.

Mass flux over the FFT-water interface was determined from the modeled scenarios (Figure 7). In the scenarios with no FFT disturbance, the mass flux was fairly constant with time. The mass fluxes generated by the scenarios with disturbances exhibited sharp increases on the days the disturbance was simulated (i.e., 15 October, both years). Mass flux from the FFT rapidly decreased afterward as the concentration within the disturbed depth was equal to the water cover concentration at this time. The mass flux then gradually increased to a rate slightly lower than before the disturbance occurred, due to the decreasing water cover concentration and subsequently lower diffusion rates (Figure 4).

The cumulative mass released per square area of FFT between May 2013 and November 2015 was determined based on the simulated mass flux over the FFT-water interface (Figure 7). The general trends for cumulative mass release, produced by the models with and without a disturbance event, were fairly similar except for the shift accompanying the disturbance. The total mass released from the FFT with a diffusion-only mass transport regime and no disturbance was very different from the diffusion models with a disturbance; however, when the mass transport regime included a greater advective flux, the relative increase in the total mass released from the FFT was not as large when a disturbance was added to the model.

The simulated Cl released during each mass balance period was determined for comparison purposes. The FFT mass release during Period 2 was substantially less than Period 1 when a disturbance was added to the model (Table 4). During Period 1, the simulated Cl release increased with the disturbance depth; however, the mass released during Period 2 did not follow this same trend. As the disturbance increased, the Cl released from the FFT generally decreased in Period 2 for all advection-dispersion transport regimes, likely due to the simulated disturbance dates. The modeled disturbances occurred on 15 October 2013 and 15 October 2014. Consequently, Period 1 included the second simulated disturbance while Period 2 had none.

Table 4. Simulated Cl Released (g m^{-2}) From the FFT During the Two Mass Balance Periods

Advective Flux (m^3 m^{-2} d^{-1})	No. Disturbance			0.5 m Disturbance			1 m Disturbance		
	Period 1	Period 2	Total[a]	Period 1	Period 2	Total[a]	Period 1	Period 2	Total[a]
0	20	18	38	47	6	53	87	6	93
0.0005	130	120	250	160	88	240	200	86	280
0.001	230	230	460	270	180	440	310	170	470
0.002	460	450	900	490	380	870	530	340	870
0.004	890	870	1760	930	810	1740	970	750	1720

[a]The mass of Cl released in both Period 1 and Period 2 for each numerical scenario.

Addition of a disturbance event during Period 2 would increase the simulated Cl release; however, the second disturbance had a smaller overall impact on the mass released from the FFT compared to the first, and so a third disturbance is also expected to be less significant.

The total mass released from the FFT, as determined by the two mass balances (296 g m^{-2} in Period 1 and 277 g m^{-2} in Period 2), was comparable to the simulated mass release over the same periods (Table 4). The results from the mass balances correspond to an advection-diffusion regime with a pore water flux between 0.001 and 0.002 m^3 m^{-2} d^{-1}. However, the mass balance sensitivity analysis indicated that the mass released from the FFT could potentially range from 200 to 395 g m^{-2} in Period 1, and 190 to 365 g m^{-2} in Period 2. The simulated pore water flux range associated with these mass flux values is 0.0005 to 0.004 m^3 m^{-2} d^{-1} (Table 4).

4. Discussion

The results from both the mass balance calculations and the numerical models confirmed that FFT was the dominant Cl source to the water cover during the study period. The numerical models provided additional insight into the main mechanisms potentially driving this mass release. Comparison of the simulations with the mass balance calculations and field observations indicate that the FFT is likely exhibiting a transient advection-dispersion mass transport regime, due to FFT settlement and shifting concentrations in the water cover over time.

Given an advective-dispersion mass transport regime, the results from the mass balances were also used to determine the FFT pore water flux associated with the calculated mass release. The pore water flux from the FFT, q (m^3 m^{-2} a^{-1}), was determined with:

$$M_{pw} = q \cdot C + n \cdot D_h \cdot \frac{\Delta C}{\Delta z} \tag{6}$$

given the calculated mass release from the FFT during each mass balance year, M_{pw} (300 g m^{-2} a^{-1} in Period 1 and 280 g m^{-2} a^{-1} in Period 2), the average Cl concentration at the FFT-water interface over the given period, C (480 g m^{-3} in Period 1 and 410 g m^{-3} in Period 2), the FFT porosity, n (0.86 m^3 m^{-3}), the hydrodynamic dispersion coefficient, D_h (0.03 m^2 a^{-1}), and the change in concentration with depth measured through the FFT, $\frac{\Delta C}{\Delta z}$ (300 g m^{-4} in Period 1 and 470 g m^{-4} in Period 2). The pore water fluxes determined from the above equation were 0.6 m^3 m^{-2} a^{-1} for Period 1 and 0.7 m^3 m^{-2} a^{-1} for Period 2, which both correspond to an approximate daily pore water flux of 0.002 m^3 m^{-2} d^{-1}. The estimated pore water flux was greater for Period 2 even though the calculated mass flux from the FFT was less than Period 1. This was likely due to the lower average concentration at the FFT-water interface during this period.

The FFT-water interface sonar surveys revealed that settlement ranged from 0 to 2 m, between October 2013 and October 2015. The area-weighted average settlement was 1.49 m over the 2 year period, or 0.75 m^3 m^{-2} a^{-1}, assuming equal settlement in both years. This value is similar to the two pore water release rates calculated from the mass balances. Thus, the assumed advection-dispersion mass transport regime and mass balance method predicted a similar pore water release as observed in the field.

The influence of mass exchange with the pit walls was not considered in this study. Exchange resulting in mass release to the water cover would have resulted in lower values for mass contribution from the FFT and the associated pore water flux. Conversely, exchange reactions causing mass removal from the water

Table 5. RMSE for Simulated Disturbance Depth Range and 0.002 $m^3\ m^{-2}\ d^{-1}$ Advection Compared to Normalized Field Concentrations (%)

Disturbance (m)	Location		
	P1	P2	P3
0.5	10.2	18.8	15.2
0.55	9.6	18.1	14.5
0.6	8.9	17.1	13.4
0.65	8.1	15.9	12.1
0.7	7.4	14.3	10.6
0.75	7.3	12.6	9.1
0.8	8.0	10.8	8.0
0.85	9.5	9.1	7.7
0.9	11.6	7.8	8.7
0.95	14.2	7.4	10.7
1.0	17.0	8.2	13.4

cover would produce greater pore water and mass release from the FFT, given the above calculations. The slight difference in the calculated pore water flux from the mass balance results and the measured area-weighted average settlement could be due to diffusion of mass from the water cover into the pit walls. However, further study is required to investigate the influence of pit wall exchange on mass in BML.

In addition to chemical mass transport via advection-dispersion, the results from the numerical models suggested that some form of FFT disturbance might also affect the water cover concentration over time. The simulated Cl profiles indicated a possible advection range, as the best fit mass flux scenario changed with the simulated disturbance depth and the exact depth of the disturbance remains unknown.

The mass balance method and area-weighted average settlement suggest that the pore water movement through the FFT was approximately 0.002 $m^3\ m^{-2}\ d^{-1}$ over the study period. The numerical models were rerun with this advective flux and varying disturbance depths between 0.5 and 1 m, to evaluate the disturbance depth providing the best fit to the measured chloride profiles (Table 5). At Platform 1, a 0.75 m disturbance provided the best fit, while 0.85 m and 0.95 m disturbances produced the lowest RMSE values for the Cl profiles from Platforms 3 and 2, respectively. Platforms 2 and 3 are closer to the shore, so these locations would likely experience greater impacts from waves, such as internal seiches, within the water cover. These results suggest that the influence of FFT disturbance on the movement of mass over the FFT-water interface likely varies with location at BML.

Overall, these findings are similar to the previous tracer investigation conducted at BML [*Dompierre and Barbour*, 2016]; however, this study demonstrates that multiple methods can be used to assess mass loading to an EPL from underlying FFT, and the mass transport mechanisms within the FFT are changing over time. The original study [*Dompierre and Barbour*, 2016] found an advective mass transport regime of 0.004 $m^3\ m^{-2}\ d^{-1}$ and a 1.1 m FFT disturbance, while this investigation observed lower values for both advection and disturbance depth. The current study covered a later time period, so the smaller advective flux could be explained by decreasing FFT settlement rates over time. In addition, disturbance within the FFT will likely decrease as the FFT-water interface elevation declines and the depth of the water cover increases. These observations indicate that mass release to the EPL water cover in later years will be predominantly through diffusion.

The methods presented in this study may be used to assess mass movement through other water bodies, and are particularly useful for systems where multiple processes influence mass transport or where conventional tracer studies are not feasible. Conducting both a mass balance of the water body and mass transport modeling through underlying sediments, provides a clearer picture of mechanisms contributing to mass flow. The use of multiple methods also helps to address issues with uncertainty in complex systems. Finally, further understanding can be gained by comparing results to general field observations (e.g., area-weighted settlement) as illustrated in this case study.

5. Conclusions

The FFT in BML is undergoing self-weight consolidation causing substantial pore water and chemical mass loading to the overlying water cover, as confirmed by both the mass balance and numerical methods used in this study. The approximate pore water release from the FFT was $4.15 \times 10^6\ m^3\ a^{-1}$ over the studied period. The estimated Cl mass release from the FFT (average of 287 $g\ m^{-2}\ a^{-1}$) was substantially larger than other mass sources (Table 1). However, the advection-dispersion mass transport regime through the FFT will change over time, as FFT settlement by self-weight consolidation is anticipated to gradually decrease.

The multiple methods employed in this study allowed for a comprehensive consideration of mass transport over the FFT-water interface. Together, the mass balances and numerical models confirmed an advection-

dispersion mass transport regime through the FFT with a seasonal disturbance ranging from 0.75 to 0.95 m at the three sample locations. The numerical simulations also provided insight on the overall effect of these disturbances on the mass loading to the water cover. Although the disturbance caused a sharp increase in mass flux over the FFT-water interface, its overall influence on the predicted cumulative mass release was relatively small, given an advection-dispersion mass transport regime. This study demonstrated the benefit of using multiple methods for assessing mass transport.

The results from the chemical mass balance highlighted the importance of operational controls on the geochemical regime within an EPL. Pumping rates (in and out) were observed to largely control the water balance. These rates will determine the water cover volume, which based on the sensitivity analysis, was an important parameter in the mass balance calculations. Future anthropogenic changes may also affect BML. For example, the BML watershed is expected to increase as more surrounding land is reclaimed. The runoff water coming from this larger watershed may have a higher dissolved solids content than those observed in this study, causing runoff to be a more significant contributor to mass in the future. Thus, future EPL design must consider the movement of water and mass through the greater reclamation landscape.

The results from this study provide an initial assessment of the geochemical regime in the BML cover, which can be used as a baseline for future studies and will assist in the development of monitoring plans at this study site. This investigation also highlights essential considerations for future EPL design, such as self-weight consolidation rates, field conditions, operational controls, and surrounding reclamation activities, as these will affect the water and chemical balances in the water cover over time. The FFT contributed substantial mass to the water cover over the monitored periods, revealing the importance of studying the geochemical characteristics of any waste material placed in an EPL or similar reclamation feature. Finally, this study highlights the need for large-scale reclamation design considering water and mass movement throughout the entire reclaimed landscape, particularly in regions like the Athabasca oil sands where large areas of land have been disturbed.

Acknowledgments

Data supporting the study conclusions can be obtained in the figures and tables provided in the manuscript. Funding was provided by Syncrude Canada Ltd. and the Natural Sciences and Engineering Research Council of Canada through the Collaborative Research and Development grants program (Grant No. CRDPJ 476388) and the Industrial Research Chairs Program (Grant No. IRCPJ 428588–11). We thank G. Halferdahl, D. Heisler, J. Lutz, and W. Zubot from Syncrude Canada Ltd., and Stephanie Villeneuve from the University of Saskatchewan, for their technical contributions to this study, and J. Price, University of Waterloo, for provision of precipitation chemistry data.

References

Allen, E. W. (2008), Process water treatment in Canada's oil sands industry: I. Target pollutants and treatment objectives, *J. Environ. Eng. Sci.*, *7*(2), 123–138.

Aubinet, M., T. Vesala, and D. Papale (2012), *Eddy Covariance: A Practical Guide to Measurement and Data Analysis*, 1st ed., Springer, New York.

Baer, T. (2014), An evaluation of the use of natural stable isotopes of water to track water movement through oil sands mine closure landforms, MSc thesis, Civ. Eng., Univ. of Saskatchewan, Saskatoon, Canada.

Baer, T., and S. L. Barbour (2013), An evaluation of the use of stable water isotopes to characterize and track water through oil sands mine closure landforms, in *66th Canadian Geotechnical Conference*, Can. Geotech. Soc.., Richmond, B. C., Canada.

Blanken, P. D., W. R. Rouse, A. D. Culf, C. Spence, L. D. Boudreau, J. N. Jasper, B. Kochtubajda, W. M. Schertzer, P. Marsh, and D. Verseghy (2000), Eddy covariance measurements of evaporation from Great Slave Lake, Northwest Territories, Canada, *Water Resour. Res.*, *36*(4), 1069–1077.

Boudreau, B. P. (1996), The diffusive tortuosity of fine-grained unlithified sediments, *Geochim. Cosmochim. Acta*, *60*(16), 3139–3142.

Canada's Oil Sands Innovation Alliance Inc. (COSIA) (2012a), Focus areas: Tailings [online], Calgary, Alberta, Canada. [Available at http://www.cosia.ca, last accessed 6 July 2016.]

Canada's Oil Sands Innovation Alliance Inc. (COSIA) (2012b), Technical guide for fluid fine tailings management [online], Calgary, Alberta, Canada. [Available at http://www.cosia.ca/initiatives/project-research, last accessed 27 July 2016.]

Carey, S. K. (2008), Growing season energy and water exchange from an oil sands overburden reclamation soil cover, Fort McMurray, Alberta, Canada, *Hydrol. Processes*, *22*(15), 2847–2857.

Carrier, D., B. Shaw, and J. Lee (2007), Syncrude West in Pit (WIP) 1995 to 2006: Consolidation modelling summary, internal report, Syncrude Canada Ltd., Fort McMurray, Alberta, Canada.

Caughill, D. L., N. R. Morgenstern, and J. D. Scott (1993), Geotechnics of nonsegregating oil sand tailings, *Can. Geotech. J.*, *30*(5), 801–811.

Chalaturnyk, R. J., J. D. Scott, and B. Özüm (2002), Management of oil sands tailings, *Petrol. Sci. Technol.*, *20*(9–10), 1025–1046.

Cox, M. H., G. W. Su, and J. Constantz (2007), Heat, chloride, and specific conductance as ground water tracers near streams, *Ground Water*, *45*(2), 187–195.

Cumulative Environmental Management Association (CEMA) (2012), End pit lakes guidance document [online], Fort McMurray, Alberta, Canada. [Available at http://www.cemaonline.ca, last accessed 26 July 2016.]

Cussler, E. L. (1997), *Diffusion—Mass Transfer in Fluid Systems*, 2nd ed., Cambridge Univ. Press, Cambridge, U. K.

Davis, S. N., G. M. Thompson, H. W. Bentley, and G. Stiles (1980), Ground-water tracers—A short review, *Ground Water*, *18*(1), 14–23.

Dompierre, K. A., and S. L. Barbour (2016), Characterization of physical mass transport through oil sands fluid fine tailings in an end pit lake: A multi-tracer study, *J. Contam. Hydrol.*, *189*(1), 12–26.

Dompierre, K. A., M. B. J. Lindsay, P. Cruz-Hernández, and G. M. Halferdahl (2016), Initial geochemical characteristics of fluid fine tailings in an oil sands end pit lake, *Sci. Total Environ.*, *156*, 196–206.

Environment Canada (2015), Canadian Climate Data [online], Gov. of Can., Ottawa. [Available at http://climate.weather.gc.ca, last accessed 10 Jan. 2016.]

Ferguson, H. L., A. D. J. O'Neill, and H. F. Cork (1970), Mean evaporation over Canada, *Water Resour. Res.*, *6*(6), 1618–1633.

Feth, J. H. (1981), Chloride in natural continental water—A review [online], *U.S. Geol. Surv. Water Supply Pap. 2176*, U.S. Geol. Surv., Reston, Va. [Available at https://pubs.er.usgs.gov/publication/wsp2176, last accessed 16 Feb. 2016.]

Gelhar, L. W., C. Welty, and K. R. Rehfeldt (1992), A critical review of data on field-scale dispersion in aquifers, *Water Resour. Res.*, *28*(7), 1955–1974.
GEO-SLOPE International Ltd. (2012), *Contaminant Modeling With CTRAN/W, Version 2012* [computer program], GEO-SLOPE Int. Ltd., Calgary, Canada.
GEO-SLOPE International Ltd. (2013), *Seepage Modeling With SEEP/W, Version 2012* [computer program], GEO-SLOPE Int. Ltd., Calgary, Canada.
Gosselin, P., S. E. Hrudey, M. A. Naeth, A. Plourde, R. Therrien, G. Van Der Kraak, and Z. Xu (2010), Environmental and Health Impacts of Canada's Oils Sands Industry, R. Soc. of Canada, Ottawa, Canada.
Government of Alberta (2014), Alberta's oil sands: Alberta's clean energy future [online], Edmonton, Canada. [Available at http://oilsands.alberta.ca/reclamation.html, last accessed 23 May 2016.]
Government of Alberta (2015), Lower Athabasca Region—Tailings Management Framework for the Mineable Athabasca Oil Sands, Gov. of Alberta, Alberta, Canada.
Government of Alberta (2016), Alberta Energy: Our business—Oil sands [online], Edmonton, Canada. [Available at http://www.energy.alberta.ca/oilsands/791.asp, last accessed 23 May 2016.]
Jacquet, N. G. (1976), Ground-water and surface-water relationships in the glacial province of northern Wisconsin—Snake Lake, *Ground Water*, *14*(4), 194–199.
Jeeravipoolvarn, S., J. D. Scott, and R. J. Chalaturnyk (2009), 10 m standpipe tests on oil sands tailings: Long-term experimental results and prediction, *Can. Geotech. J.*, *46*(8), 875–888.
Kamp, G. L. D. van der , Luba, J. A. Cherry, and H. Maathuis (1994), Field study of a long and very narrow contaminant plume, *Ground Water*, *32*(6), 1008–1016.
Kasperski, K. L., and R. J. Mikula (2011), Waste streams of mined oil sands: Characteristics and remediation, *Elements*, *7*(6), 387–392.
Kavanagh, R. J., R. A. Frank, K. D. Oakes, M. R. Servos, R. F. Young, P. M. Fedorak, M. D. MacKinnon, K. R. Solomon, D. G. Dixon, and G. Van Der Kraak (2011), Fathead minnow (*Pimephales promelas*) reproduction is impaired in aged oil sands process-affected waters, *Aquat. Toxicol.*, *101*(1), 214–220.
Lawrence, G. A., E. W. Tedford, and R. Pieters (2016), Suspended solids in an End Pit Lake: Potential mixing mechanisms, *Can. J. Civ. Eng.*, *43*(3), 211–217.
Lee, D. R., J. A. Cherry, and J. F. Pickens (1980), Groundwater transport of a salt tracer through a sandy lakebed, *Limnol. Oceanogr.*, *25*(1), 45–61.
Li, Y. H., and S. Gregory (1974), Diffusion of ions in sea-water and in deep-sea sediments, *Geochim. Cosmochim. Acta*, *38*, 703–714.
Masliyah, J., Z. Zhou, Z. Xu, J. Czarnecki, and H. Hamza (2004), Understanding water-based bitumen extraction from Athabasca Oil Sands, *Can. J. Chem. Eng.*, *82*(4), 628–654.
Murray, W. A. (1981), The 1981 Snowpack Survey in the AOSERP Study Area, Alberta Environ., Res. Manage. Div., Gov. of Alberta, Edmonton, Canada.
Osacky, M., M. Geramian, D. G. Ivey, Q. Liu, and T. H. Etsell (2013), Mineralogical and chemical composition of petrologic end members of Alberta oil sands, *Fuel*, *113*, 148–157.
Oswald, C. J., and W. R. Rouse (2004), Thermal characteristics and energy balance of various-size Canadian Shield lakes in the Mackenzie River Basin, *J. Hydrometeorol.*, *5*(1), 129–144.
Penman, H. L. (1948), Natural evaporation from open water, bare soil and grass, *Proc. R. Soc. London, Ser. A*, *193*, 120–145.
Prakash, S., J. A. Vendenberg, and E. Buchak (2011), The oil sands pit lake model—Sediment diagenesis module, in *19th International Congress on Modelling and Simulation, Modelling and Simulation Society of Australia and New Zealand, Perth, Australia*, edited by F. Chan, D. Marinova, and R. S. Anderssen, pp. 3761–3767, Modell. and Simul. Soc. of Aust. and N. Z., Canberra.
Rimmer, A., Y. Aota, M. Kumagai, and W. Eckert (2005), Chemical stratification in thermally stratified lakes: A chloride mass balance model, *Limnol. Oceanogr. Methods*, *50*(1), 147–157.
Rouse, W. R., C. M. Oswald, J. Binyamin, P. D. Blanken, W. M. Schertzer, and C. Spence (2003), Interannual and seasonal variability of the surface energy balance and temperature of central Great Slave Lake, *J. Hydrometeorol.*, *4*(4), 720–730.
Sacks, L. A., A. Swancar, and T. M. Lee (1998), Estimating ground-water exchange with lakes using water-budget and chemical mass-balance approaches for ten lakes in ridge areas of Polk and Highlands Counties, Florida [online], *U.S. Geol. Surv. Water-Resour. Invest. Rep. 98–4133*, U.S. Geol. Surv., Reston, Va. [Available at https://pubs.er.usgs.gov/publication/wri984133, last accessed 16 Feb. 2016.]
Suthaker, N. N., and J. D. Scott (1996), Measurement of hydraulic conductivity in oil sand tailings slurries, *Can. Geotech. J.*, *33*(4), 642–653.
Weiner, E. R. (2013), *Applications of Environmental Aquatic Chemistry: A Practical Guide*, 3rd ed., Taylor and Francis Group, Boca Raton, Fla.